2019 32nd International Conference on VLSI Design and 2019 18th International Conference on Embedded Systems (VLSID)

Design of Continuous-Flow Lab-on-Chip with 3D Microfluidic Network for Sample Preparation

Tapalina Banerjee
ACM Unit
Indian Statistical Institute
Kolkata, India
tapalinabanerjee1@gmail.com

Sudip Poddar
ACM Unit
Indian Statistical Institute
Kolkata, India
sudippoddar2006@gmil.com

Sarmishtha Ghoshal
School of VLSI Tech.
IIEST, Shibpur
Kolkata, India
sharmi.bhatta@gmail.com

Bhargab B. Bhattacharya
ACM Unit
Indian Statistical Institute
Kolkata, India
bhargab.bhatta@gmail.com

***Abstract*—Microfluidic labs-on-chip have fueled the automation of biochemical protocols (assays) on a tiny device and found versatile applications to DNA analysis, medical diagnostics, forensics, and drug design. Sample preparation, which includes dilution of fluids or solution mixing, is needed as a preprocessing step for most of the assays. Although continuous-flow microfluidic biochips (CFMB) are being widely used by chemists and biologists, accurate sample preparation with them is a challenge and the technology lacks an automated CAD-tool that can be deployed to design the underlying fluidic network. In this paper, we present, the physical design of a 3D-fluidic network that can be used as a universal platform for dilution preparation. The network does not need any control-valve for fluid navigation or multiplexing, yet it is fully programmable. A sample with any given concentration factor (*CF*) can be produced as output-flow by controlling only the rate of input-fluid injection. Simulation with COMSOL Multiphysics Software shows that the proposed free-flowing CFMB outperforms prior approaches in achieving the accuracy of *CF*s and diversity of applications.**

***Index Terms*—design automation, microfluidic lab-on-chip**

I. Introduction

Advances in microfluidic technologies over the last few decades have led to the development of Lab-on-Chip (LoC) devices that provide a multitude of fluidic functions on a single chip. They are increasingly replacing bulky and expensive biochemical bench-top procedures needed in hospitals, research labs, or at point-of-care (PoC) stations. Embedded systems built with these chips provide quick and low-cost solutions to sample preparation, DNA analysis, drug design, pathological diagnostics, cell sorting, therapeutics, and synthetic biology to name a few [1], [2]. Two major classes of LoCs are primarily used in practice: droplet-based digital microfluidic biochips (DMFBs), and continuous-flow microfluidic biochips (CFMBs). While several computer-aided design (CAD) tools have already been developed for DMFBs, very few are available for the latter class. CFMBs are historically more preferred in the biochemistry community to implement various assays and detection [3]–[5]. Additionally, no tools are available for automating the physical design of 3D-channels that define the underlying fluidic architecture of a CFMB.

T. Banerjee and S. Poddar are working as doctoral candidate at the CSE Dept., University of Calcutta (as CSIR Senior Research Fellow), and at the School of VLSI Tech., IIEST, Shibpur (as CSIR Research Associate), respectively. The work of B. B. Bhattacharya, was supported, in part, by INAE Chair Professorship and by the DST-SERB Research Grant No. EMR/2016/005977.

CFMBs are usually fabricated with two technologies. One approach is to use a multi-layer planar technology consisting of a flow layer and a control layer. In the flow layer, fluids are channelled through pre-etched micro-network, whereas the flow is controlled by opening and closing of micro-valves manipulated via control layer. Micro-pumps are used in both layers to produce pressure gradients with fluid or air. Fluidic networks of these chips are typically customized for specific applications. Today's biochips use more than 25,000 valves to implement large-scale and concurrent experiments [6]. However, the performance of micro-valves is highly sensitive to channel layout and pressurization scheme. For example, pressure gradient in a PDMS micro-channel may become feeble due to its expansion [7], leading to a number of specific design concerns such as slow response time and asynchronous valve actuation [6], [8]. This technology has also been used recently to build general-purpose field-programmable valve-array (FPVA) [9], which resembles a regular 2D-array of channels, where valves are inserted at every junction to control fluid-flow. More complex units such as mixer, separator, detector, multiplexers, and storage-units can be built by the combination of channels and valves [10]. Although the use of control layer brings the benefit of programmability, these chips suffers from various defects caused by the degradation and hysteresis of elastic channels and valves [11], [12].

A second and simpler technology for designing CFMBs is to use *free-flowing* fluid through rigid channels, where no control layer or valves are needed. A switching mechanism is used only to inject or stop fluid-flow at the input ports. The flow is controlled solely by the global fluidic (hydraulic) resistance of the channels and injection rates. Traditionally, these chips are more popular among biochemists, as they are inexpensive and easy to fabricate. Free-flowing chips are, however, fully customized and cannot be re-programmed for general usage. Furthermore, since there is almost no control on fluid navigation, it is difficult to implement protocols such as dilution or mixture preparation, which require both high degree of flexibility and precision on concentration factors (CF).

Sample preparation is required as a pre-processing step in biochemical protocols, which includes, among others, dilution of a fluid sample to a desired CF. Albeit it can be prepared very accurately using DMFBs [2], [13], no attempt has yet

2380-6923/19/$31.00 ©2019 IEEE
DOI 10.1109/VLSID.2019.00052

been made to achieve the same level accuracy in target-CF while using free-flowing CFMBs. In the past, only a few work using 1D/2D fluidic networks were proposed for sample preparation using CFMBs [14]–[18]. Moreover, they suffer from non-programmability, loss of costly reagents, high latency, and inability to sustain a steady flow with the target-*CF*. Some results on programmable fluidic networks for sample preparation have also been reported using valve-based CFMBs [5], [19] based on 2D-channel modeling.

With the advent of 3D-printed CFM-chips, achieving precise control on channel geometries has now become tenable. In this paper, we propose, for the first-time, a programmable 3D fluidic network for dilution preparation using only free-flowing technology. We suitably adapt a dilution algorithm previously used for DMFBs [20] to map it on CFMBs, and build a CAD tool to automate the design flow. We analyze the network based on electrical and hydraulic modeling, and present a complete physical design of the chip layout. Extensive simulation with COMSOL Multiphysics Software [21] shows output flow having early convergence and sustained stability of the target-*CF* with high accuracy. The error bound in target-*CF* obtained by the proposed *LoC* matches with the best bound so far achievable using only digital microfluidic chips.

II. Automated Sample Preparation

Algorithmic sample preparation with LoCs requires a sequence of mix/split operations between two or more fluidic reagents. In dilution, sample and buffer fluids are mixed in a given volumetric ratio to achieve a desired target concentration factor (*CF*, $0 \leq CF \leq 1$) of the sample [2], [13]. The *CF* of raw sample (neutral buffer) is considered as 1 (0). Most of the sample-preparation algorithms use the (1:1) mixing-model where a mix operation is performed between two unit-volume fluids followed by a balanced splitting into two equal unit-volume components; for example, if a unit-volume fluid with *CF* = C_1 is mixed with another unit-volume fluid with *CF* = C_2, then after the mix-split operation, the *CF* of each sister component becomes $\frac{C_1+C_2}{2}$. Given a target-*CF*, a specific sequence of such mix-split operations is required to reach the target-*CF* using sample and buffer fluids [2], [13]. In general, the complete dilution process can be envisaged as a directed acyclic graph, known as *mix-split graph/tree*, which provides a sequence of (1:1) mix-split operations to be performed for generating the desired target-dilution. The depth *n* ($n > 0$) of the mix-split graph, which is determined by a user-specified error-tolerance limit ϵ ($0 \leq \epsilon < 1$), denotes the accuracy of the target-*CF*. Because of the use of (1:1) mixing model, each *CF* is represented as $\frac{x}{2^n}$ (*n* is a positive integer, and *x* is a non-negative integer such that $0 \leq x \leq 2^n$), and hence, the error limit in CF becomes $\frac{1}{2^{n+1}}$. A choice of *n* =10 (i.e., 10 mix-split steps) ensures very negligible error ($\frac{1}{2^{11}} \simeq 0.000488281$) in sample preparation [2]. Hence, for this case, the target-*CF* range from 0%-100% is discretized as $\frac{0}{1024}$, $\frac{1}{1024}$, $\frac{2}{1024}$, …, $\frac{1023}{1024}$, $\frac{1024}{1024}$.

An algorithm called REactant MInimization Algorithm (REMIA) was developed by Huang et al. [20] for minimizing reactant-cost while diluting a fluid sample using DMFBs. Given a target concentration factor (tCF), the mix-split sequence is described with two trees: exponential dilution tree (EDT), which produces all prime concentration values (PCVs), and skewed mixing tree (SMT), which produces tCF. The PCVs can be generated by mixing buffer with sample iteratively, i.e., their CF-values are in geometric progression $1, \frac{1}{2}, \frac{1}{4}, \cdots, \frac{1}{2^n}$. PCVs are fed to the SMT as input to produce the desired tCF. Fig. 1 shows both the trees for *tCF* = $\frac{241}{512}$. Following each $(1:1)$ mix-split step, one sister droplet is used for the next operation while the other is left as waste.

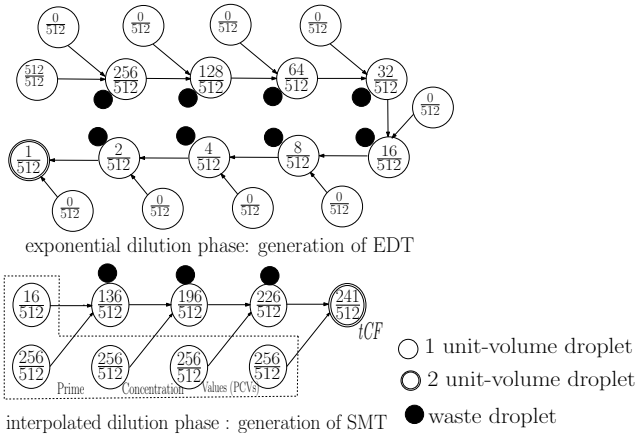

Fig. 1. Example of REMIA in DMFB

III. Motivation

Although several CAD-algorithms for sample preparation with CFMBs have been reported in the past [5], [14], [18], [19], no simulation validating real-life 3D fluid dynamics through micro-channels has been made so far. A few studies based on 2D-modeling of channels have been reported for valve-based CFMBs [19] and for free-flowing CFMBs [14]. Note that the results based on 2D modeling of fluid flow, mixing, diffusion, or turbulence cannot truthfully reflect the 3D analog reality [22]. Additionally, achieving proper mixing of two or more fluids in micro-channels on-the-fly is a challenging task since the flow through them is set as laminar causing viscous effects [23]. In CFMBs, mixing is predominantly performed via molecular diffusion, which is time-consuming [24]. Use of passive or active mixers can expedite mixing and the former type is preferred as they are easy to fabricate [22], [23], [25]. For real-life 3D micro-channels in CFMBs, there exists neither any truthful simulation nor any procedure for designing a programmable diluter with details of channel and mixer architectures.

The above shortcomings motivate us to propose a complete physical design of a programmable 3D free-flowing microfluidic LoC, which can be used to implement fluid dilution of any tCF. In order to perform mixing operations more homogeneously, we use 3D Y-shaped serpentine micro-channels with periodic in-flow obstacles (C-shaped) that facilitate intensive fluid stirring and swirling vortices [23]. Such microfluidic channels can be manufactured using different micro-fabrication techniques [25].

IV. Theoretical Groundwork

A 2D model of a free-flowing CFMB that is used for dilution was presented in [14] based on bit-scan algorithm [13], which requires only sample and buffer as input fluids. In the proposed work, we adapt REMIA on a 3D free-flowing fluidic architecture by implementing PCV and tCF production, in two independent steps. Since no control valve is used in the network, no split operation is executed as in REMIA; instead, a mix-split step is emulated by doubling the flow-rate at every next inlet. As a sequel, the waste-management issue, which is an integral part of all DMFB-based sample-preparation algorithms, does not arise here. Instead of producing waste, the method outputs the entire flow with the desired dilution. The dynamics of fluid-flow through 3D microfluidic channels can be studied using Hagen-Poiseuille law [26] and Ohm's law. Hagen-Poiseuille equation correlates pressure drop in a fluid flowing through a long pipe with its volumetric flow rate, and is applicable to Newtonian fluids with laminar flow through a rigid channel of constant cross-section. In the steady-state, velocity field in the fluidic channel is unidirectional, laminar, and without acceleration. For a microfluidic network with rectangular cross-section,

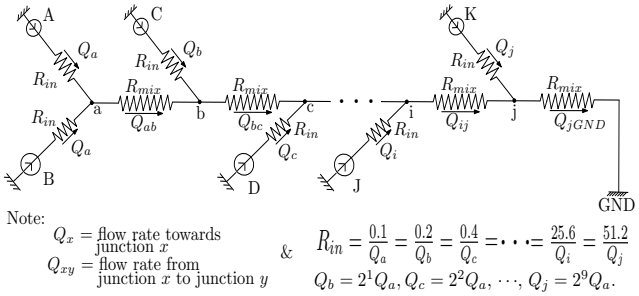

Fig. 2. Schematic diagram

the hydraulic resistance of the microchannel (R_{hyd}) can be expressed by combining Hagen-Poiseuille flow and Ohm's law. The R_{hyd} [26] is given by:

$$R_{hyd} = \frac{8\mu l(w+h)^2}{h^3 w^3} \tag{1}$$

where, the symbols are described in Table I. The resistive

TABLE I
Symbolic Notation

Symbol	Stands for
μ	coefficient of viscosity
h	height of the microchannel
l	length of the microchannel
w	width of the microchannel
Q	flow rate (volume per time) of the fluid
R_{hyd}	hydraulic resistance of a microchannel
R_{in}	hydraulic resistance of inlet-side microchannel
R_{mix}	hydraulic resistance of mixing microchannel
Re	Reynolds number
ρ	density of the fluid
u	fluid-injection rate

behavior of fluid-flow can be captured by an equivalent electrical network as depicted in Fig. 2. Since we consider rigid

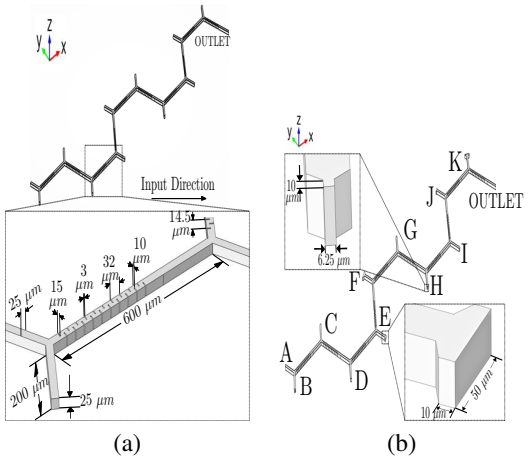

Fig. 3. COMSOL Modeling of Microfluidic Network

channels, no capacitor element is needed in the circuit. We simulate the electrical circuit considering hydraulic resistance of the channel, flow rate and fluid injection pressure as resistor, current, and applied voltage, respectively, and analyze it by applying Kirchhoff's laws (KCL and KVL) and Ohm's law at each fluidic junction. Note that fluid-injection rates are chosen in geometric progression (with a multiplying factor of two). We consider (i) low-valued hydraulic resistance for inlet micro-channels (R_{in}), and high-valued hydraulic resistance for mixing micro-channels (R_{mix}), which are assumed to be constant throughout the network, and (ii) we do away with the split operation of the $(1:1)$ mix-split model by doubling fluid-injection rate at each subsequent inlet port following a mixing junction. We also choose a low value (< 2300) of Reynolds number (Re), a dimensionless parameter, so as to ensure laminar flow of fluid through the channels [26]. Note that Re can be computed by dividing inertial force by viscous force μ as follows:

$$Re = \frac{Inertial\ force}{Viscous\ force} = \frac{\rho u l}{\mu} \tag{2}$$

In order to ensure uniform flow for Newtonian fluids through the micro-channels against viscous forces, geometrical similarity must be preserved at flow-boundaries, and Reynolds number should be the same throughout the network [26], [27].

V. Proposed 3D Fluidic Network

The overall geometric architecture of the proposed 3D free-flowing microfluidic diluter is shown in Fig. 3. It is built as a linear chain of Y-junctions (to enable confluence of two incoming flows), and straight channels (to enable mixing), each having a uniform rectangular cross-section. The details of their physical dimensions are shown in the figure. The microfluidic network is designed in accordance with Expression (1) and Expression (2), and is validated on the basis of its equivalent electrical circuit as shown in Fig. 2. As discussed in Section II, the length of the linear microfluidic array need not exceed 10 for achieving high accuracy in CF. Note that the number of Y-shaped junctions used in the array should be less than

or equal to the depth (n) of the skewed mixing tree generated by REMIA, and typically, $n \leq 10$.

In order to achieve quick and homogeneous mixing of fluid through a straight micro-channel, we use a linear array of passive serpentine mixers [28], comprising inter-digitized rectangular obstacles, placed orthogonally against the direction of flow in the interior of the channel. Based on the channel dimension, the turning radius [29] around an obstacle is chosen $6.5\mu m$. Such a design ensures satisfactory convective/diffusive mixing of fluids through the diluter network.

As discussed earlier, the rate of fluid injection has to be doubled at every next inlet port in the linear array. In order to avoid the need for having very large injection velocities at the rear end of the array, we use five different inlet cross-sections and two different injection rates, with values in each category progressing geometrically (see Table II). As shown in Fig. 3(b) and Table II, we apply the same resulting fluid-injection rate (0.1 mm/sec) for Inlet A and Inlet B; it increases in geometric progression with a factor two at each subsequent inlet port along the array. It is easy to show that the value of Reynolds number (Re) will remain the same along the entire flow. To double the cross-section of an inlet, a specially designed tapered rectangular union is used with the same height as shown in Fig. 3(b).

TABLE II
FLUID INJECTION RATE APPLIED AT DIFFERENT INLETS

Inlet label in Fig. 3(b)	Inlet width in μm[1]	Applied fluid injection velocity (in *mm/sec*)	Resultant rate at inlet arm (in *mm/sec*)
A,B:	6.25	0.8	0.1
C:	12.5	0.8	0.2
D:	25	0.8	0.4
E:	50	0.8	0.8
F:	100	0.8	1.6
G:	6.25	25.6	3.2
H:	12.5	25.6	6.4
I:	25	25.6	12.8
J:	50	25.6	25.6
K:	100	25.6	51.2

[1]heights are same as 25 μm

Since the proposed microfluidic network is designed as a linear array, pressure-driven fluid-injection timing at every inlet plays an important role to enable concurrent arrival of two incoming flows at Y-junctions. A deviation from this condition will badly affect the mixing ratio as well as convergence time. We calculate injection-timing based on the delay caused by hydraulic resistance, and the results are shown at Table III. Additionally, the dimensions of the fluidic network are chosen in such a way that the Reynolds number (Re) throughout the entire channel becomes less than 2000, thus warranting laminar flow of two miscible fluids [26].

TABLE III
FLUID INJECTION TIMING

Inlet [Fig. 3]	Injection time in *sec*
A,B	0
C	11
D	14
E	16
F	18
G	20
H	22
I	24
J	26
K	28

VI. SIMULATION FRAMEWORK

In order to study the flow dynamics in the proposed 3D microfluidic network, we simulate it using COMSOL Multiphysics Software [21]. The structural description of the fluidic network and dimensions of different channels are provided as inputs to the simulator. The physical parameters of various sample and buffer fluids are given in Table IV. Fig. 4 depicts a snapshot of the flow for $tCF = (\frac{241}{512})$ with accuracy $n = 9$. Initially, fluidic channels are filled-up with air. In our experiments, we have used water as buffer, and three different fluids as sample (ethanol, glycerol and *n*-pentane). The samples have different physical properties, e.g., density, viscosity (dynamic and kinematic), diffusion coefficient, conductivity (electrical and thermal), and surface tension. To study the velocity and pressure profiles of the flow in the micro-channels, we consider the single-phase laminar flow (SPF) in COMSOL [21]. The concentration profiles of the fluid-mixture at different points of the diluter network are derived based on transport-of-diluted-species (TDS) physics. For analysis of fluid dynamics, SPF uses the Navier-Stokes equation that captures the conservation of momentum [27]. For incompressible Newtonian fluid, the Navier-Stokes equation is given by:

$$\rho(\frac{\delta u}{\delta t} + u \cdot \bigtriangledown u) = -\bigtriangledown p + \bigtriangledown \cdot (\mu(\bigtriangledown u + (\bigtriangledown u)^T) - \frac{2}{3}\mu(\bigtriangledown \cdot u)I) + F \quad (3)$$

where *p* is the fluid pressure in the microchannel, *F* stands for the applied external forces on fluids and all other variables are same as previously mentioned. Inertial forces are represented by the left hand side. Pressure force and viscous force are denoted by $(- \bigtriangledown p)$ and $(\bigtriangledown \cdot (\mu(\bigtriangledown u + (\bigtriangledown u)^T) - \frac{2}{3}\mu(\bigtriangledown \cdot u)I))$, respectively. The above mentioned equation is solved along with the continuity equation [26]:

$$\frac{\delta \rho}{\delta t} + \bigtriangledown \cdot (\rho \mu) = 0 \quad (4)$$

which represents the mass conservation.

Based on Fick's laws, the physics TDS solves the convection-diffusion equation [27]. TDS also uses the transport equation:

$$\bigtriangledown(-D_i \cdot \bigtriangledown c_i) + u \cdot \bigtriangledown c_i = R_i \quad (5)$$

where the diffusion co-efficient of i^{th} fluid is D_i, concentration of i^{th} fluid is c_i and R_i represents the reaction rate of fluids. We have performed our experiments with three different samples - ethanol (diffusivity 1.24×10^{-9} m^2/sec), glycerol (diffusivity 0.94×10^{-9} m^2/sec), and *n*-pentane (diffusivity 0.000807 m^2/sec). Water is used as buffer.

The computational domain is set by specifying surface boundary conditions; they affect velocity, pressure and concentration factor in the channels. We use a coarse grid size for meshing in straight channels, and a finer grid with higher granularity for Y-junctions. In order to study flow dynamics

with time, we consider a scale in units of second, and perform simulation for the interval 0 *sec* to 50 *sec* with a time-step of 1 *sec*. The details of our computational platform are provided in Table IV.

TABLE IV
COMPUTATION PLATFORM

CPU	Intel Core $i7-3770$CPU @ 3.40 GHz, 4 cores
Operating System	Windows 10
Software	COMSOL Multiphysics 5.2
Model Dimension	3D
Materials (incompresible Newtonian Fluid)	Water used as buffer Sample: Diffusion co-efficient of sample in water $[m^2/sec]$ Ethanol: 1.24×10^{-9} Glycerol: 0.94×10^{-9} *n*-pentane: 0.000807
Physics	Laminar flow (SPF: Single-Phase Flow) Transport of Diluted Species (TDS)
Meshing	Predefined element size at extra fine while calibrating fluid dynamics
Study	Time dependent (Time range: 0 *sec* - 50 *sec*; time step 1 *sec*)

VII. RESULTS AND DISCUSSIONS

The proposed microfluidic architecture serves as a universal diluter platform. It can be used to produce the PCVs and any tCF following the *REMIA* algorithm [20]. For the former, we use only sample and buffer as input fluids. For the latter, we feed selected PCVs as inputs depending on the given tCF. The selection of PCVs and their sequencing (i.e., mapping between PCVs and inlet ports) are determined by the *REMIA* algorithm, as stated earlier. This 3D-network can be used to emulate the bit-scan algorithm [13], [14] for producing dilution. In first part of our experiment, COMSOL simulation shows that all PCVs are generated within the allowable error range of CF-accuracy, i.e., $\frac{1}{2^{n+1}}$. Table V summarizes these

TABLE V
PCV VALUES FOR ACCURACY 10

Theoretical value	$\frac{512}{1024}$	$\frac{256}{1024}$	$\frac{128}{1024}$	$\frac{64}{1024}$	$\frac{32}{1024}$
Simulated Result	$\frac{512.22}{1024}$	$\frac{255.73}{1024}$	$\frac{128.48}{1024}$	$\frac{63.7}{1024}$	$\frac{32.49}{1024}$
Theoretical value	$\frac{16}{1024}$	$\frac{8}{1024}$	$\frac{4}{1024}$	$\frac{2}{1024}$	$\frac{1}{1024}$
Simulated Result	$\frac{16.47}{1024}$	$\frac{8.49}{1024}$	$\frac{3.61}{1024}$	$\frac{2.34}{1024}$	$\frac{1.02}{1024}$
Remark:	All are within allowable error range, i.e., $\pm\frac{0.5}{1024}$				

results. Next, we generate a given tCF by using the required subset of PCVs, The COMSOL simulation for concentration profile of $tCF = (\frac{241}{512})$ is shown in Fig. 4. . For a number of tCFs we run COMSOL on the proposed architecture using both *REMIA* and the 3D-version of bit-scan algorithm [14], and observed the CF of the output flow. As reported in Table VI , all tCFs have been generated within the allowable error-

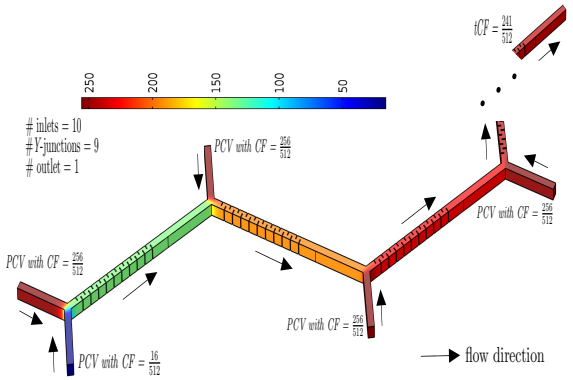

Fig. 4. COMSOL-view of concentration profile of $tCF = \frac{241}{512}$

TABLE VI
TARGET CONCENTRATION FACTORS (tCF)

Theoretical value	Simulated Result for 3D version of [14]	Simulated Result of our method
$\frac{83}{512}$	$\frac{83.1}{512}$	$\frac{83.05}{512}$
$\frac{112}{512}$	$\frac{112.3}{512}$	$\frac{112.08}{512}$
$\frac{241}{512}$	$\frac{241.5}{512}$	$\frac{241.1}{512}$
$\frac{389}{512}$	$\frac{388.88}{512}$	$\frac{389.09}{512}$
$\frac{461}{512}$	$\frac{460.89}{512}$	$\frac{461.01}{512}$

range when *REMIA* is used on the proposed 3D-diluter. In the bar-diagram of Fig. 5, we show the error in CF for

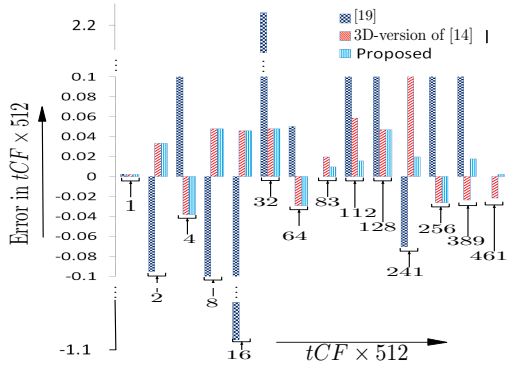

Fig. 5. Error profiles of different tCFs obtained by [19], 3D-version of [14], and the proposed method for accuracy = 9.

various targets as obtained by an earlier valve-based FPVA [19], 3D-version of [14], and the proposed method. The results demonstrate the superiority of our method in terms of accuracy in target-CF. For a particular $tCF = \frac{112}{512}$, we show in Fig. 6 that the convergence of concentration profile (with respect to time) for our method is much better than that for the 3D-version of [14]. Fig. 7 shows a snapshot of the COMSOL-view of the laminar flow through the proposed microfluidic network. For all three samples (ethanol, glycerol, *n*-pentane), we have obtained the same results as shown in Table V and Table VI.

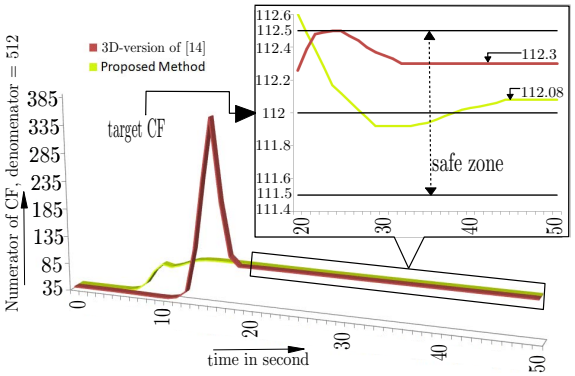

Fig. 6. Concentration profiles of $tCF=\frac{112}{512}$ generated by 3D-version of [14] and the proposed method

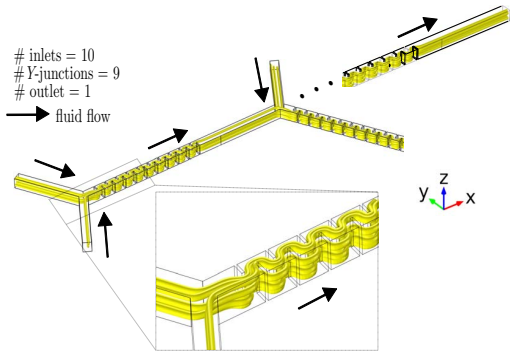

Fig. 7. Laminar streamline profile: COMSOL-view

VIII. Conclusion

In this paper, we have proposed, for the first time, the design of a free-flowing 3D microfluidic LoC network for sample preparation. The architecture is simple as it does not need any control valve. It simply enables free-flowing fluids to move through a channel-network of junctions and mixers under the control of pressure-gradients at inputs. It provides a universal diluter platform, that is, it can be programmed to produce dilution of an input fluid with any given concentration factor. The design requires at most ten *Y*-junctions, five different-size inlet ports and two different values of injection rate, in order to achieve a small error ($\leq \frac{1}{2^{11}}$) in target-*CF*. The size of the microfluidic network can be reduced if the error bound is relaxed. We present the details of physical design for the microfluidic networks, and COMSOL simulation shows that dilution is achieved with very high degree of accuracy. Compared to other continuous-flow LoCs, we have obtained faster convergence and improved accuracy. Although we have used REMIA [20] as the primary algorithm, the design can be extended or modified to accommodate other sample-preparation techniques. This study is left as a future research problem.

References

[1] C. D Chin, V. Linder, and S. Sia, "Commercialization of microfluidic point-of-care diagnostic devices," *Lab Chip*, vol. 12, no. 12, pp. 2118–2134, 2012.

[2] S. Roy, B. Bhattacharya, and K. Chakrabarty, "Optimization of dilution and mixing of biochemical samples using digital microfluidic biochips," *IEEE TCAD*, vol. 29, no. 11, pp. 1696 – 1708, 2010.

[3] J. M. Perkel, "Microfluidics: Bringing new things to life science," *Science*, vol. 322, pp. 975–977, 2008.

[4] J. Marlin and S. Quake, "Microfluidic large-scale integration: The evolution of design rules for biological automation," *Annu. Rev. Biomol. Struc.*, vol. 36, pp. 213–231, 2007.

[5] S. Bhattacharjee, S. Poddar, S. Roy, J. D. Huang, and B. B. Bhattacharya, "Dilution and mixing algorithms for flow-based microfluidic biochips," *IEEE TCAD*, vol. 36, no. 4, pp. 614–627, 2017.

[6] K.-H. Tseng, S.-C. You, J.-Y. Liou, and T.-Y. Ho, "A top-down synthesis methodology for flow-based microfluidic biochips considering valve-switching minimization," *in Proc. ACM ISPD*, pp. 123–129, 2013.

[7] A. T. H. Lau, H. M. Yip, K. C. C. Ng, X. Cui, and H. W. Lam, Raymond, "Dynamics of microvalve operations in integrated microfluidics," *Micromachines*, vol. 5, no. 1, pp. 50–65, 2014.

[8] K. Hu, T. A. Dinh, T. Ho, and K. Chakrabarty, "Control-layer routing and control-pin minimization for flow-based microfluidic biochips," *IEEE TCAD*, vol. 36, no. 1, pp. 55–68, 2017.

[9] L. M. Fidalgo, "A software-programmable microfluidic devie for automated biology," *Lab Chip*, vol. 11, no. 9, pp. 1612–1619, 2011.

[10] A. Z. Lim, Y. C. Kouzani and W. Duan, "Lab-on-a-chip: a component view," *Microsystem Technologies*, vol. 16, no. 12, pp. 1995–2015, 2010.

[11] C. Liu *et al.*, "Testing microfluidic fully programmable valve arrays (FPVAs)," in *Proc. DATE*, 2017, pp. 91–96.

[12] K. Hu, B. B. Bhattacharya, and K. Chakrabarty, "Fault diagnosis for leakage and blockage defects in flow-based microfluidic biochips," *IEEE TCAD*, vol. 35, no. 7, pp. 1179–1191, 2016.

[13] W. Thies, J. P. Urbanski, T. Thorsen, and S. P. Amarasinghe, "Abstraction layers for scalable microfluidic biocomputing," *Natural Computing*, vol. 7, no. 2, pp. 255–275, 2008.

[14] T. Banerjee, S. Ghoshal, and B. B. Bhattacharya, "Comsol-based design and validation of dilution algorithm with continuous-flow lab-on-chip," *INAE Letters (Springer)*, vol. 2, no. 2, pp. 55–63, 2017.

[15] T. Ahmed *et al.*, "Bacterial chemotaxis in linear and nonlinear steady microfluidic gradients," *Nano Letters*, vol. 10, no. 9, pp. 3379–3385, 2010.

[16] J. Atencia, G. A. Cooksey, and L. E. Locascio, "A robust diffusion-based gradient generator for dynamic cell assays," *Lab Chip*, vol. 12, no. 2, pp. 309–316, 2012.

[17] M. A. Qasaimeh, T. Gervais, and D. Juncker, "Microfluidic quadrupole and floating concentration gradient," *Nature Communications*, vol. 2, p. 464, 2011.

[18] N. L. Jeon *et al.*, "Generation of solution and surface gradients using microfluidic systems," *Langmuir*, vol. 16, no. 22, pp. 8311 – 8316, 2000.

[19] J. Wang, P. Brisk, and W. H. Grover, "Random design of microfluidics," *Lab Chip*, vol. 16, no. 21, pp. 4212–4219, 2016.

[20] J.-D. Huang, C.-H. Liu, and T.-W. Chiang, "Reactant minimization during sample preparation on digital microfluidic biochips using skewed mixing trees," in *Proc. of ICCAD*, 2012, pp. 377–383.

[21] "COMSOL Multiphysics Software." [Online]. Available: https://www.comsol.co.in/

[22] B. Olson and J. Greenough, "Comparison of two- and three-dimensional simulations of miscible richtmyer-meshkov instability with multimode initial conditions," *Physics of Fluids*, vol. 26, no. 10, 2014.

[23] S. Das, B. Kumar Patawari, P. Patowari, and S. Halder, "Computational analysis for mixing of fluids flowing through micro-channels of different geometries," in *Proc. of AIMTDR*, 2014, pp. 236:1–236:6.

[24] H. Wang, I. Pio, H. Erol, and M. Syed, "Numerical investigation of mixing in microchannels with patterned grooves," *J. Micromechanics and Microengineering*, vol. 13, no. 6, 2003.

[25] R. H. Liu *et al.*, "Passive mixing in a three-dimensional serpentine microchannel," *J. MEMS*, vol. 9, no. 2, pp. 190–197, 2000.

[26] H. A. Stone, *Introduction to Fluid Dynamics for Microfluidic Flows*. Boston, MA: Springer US, 2007, pp. 5–30.

[27] J. Crank, *The Mathematics of Diffusion*, 2nd ed. Clarendon Press Oxford [England], 1975.

[28] T. J. Ober, D. Foresti, and J. A. Lewis, "Active mixing of complex fluids at the microscale," *PNAS*, vol. 112, no. 40, pp. 12 293–12 298, 2015.

[29] A. S. Kane *et al.*, "Microfluidic mixers for the investigation of rapid protein folding kinetics using synchrotron radiation circular dichroism spectroscopy," *Anal. Chem.*, vol. 80, no. 24, pp. 9534–9541, 2008.